Wave-Number Spectra and Intermittency in the Terrestrial Foreshock Region

Y. Narita* and K.-H. Glassmeier†

Institute of Geophysics and Extraterrestrial Physics, Mendelssohnstrasse 3, D-38106 Braunschweig, Germany

R. A. Treumann‡

Department of Geoscience, Geophysics Section, Ludwig-Maximilians-University Munich, Theresienstrasse 41, D-80333 Munich, Germany

(Received 14 November 2005; published 8 November 2006)

Wave-number spectra of magnetic field fluctuations are directly determined in the terrestrial foreshock region (upstream of a quasiparallel collisionless shock wave) using four-point Cluster spacecraft measurements. The spectral curve is characterized by three ranges reminiscent of turbulence: energy injection, inertial, and dissipation range. The spectral index for the inertial range spectrum is close to Kolmogorov's slope, $-5/3$. On the other hand, the fluctuations are highly anisotropic and intermittent perpendicular to the mean magnetic field direction. These results suggest that the foreshock is in a weakly turbulent and intermittent state in which parallel propagating Alfvén waves interact with one another, resulting in the phase coherence or the intermittency.

DOI: 10.1103/PhysRevLett.97.191101 PACS numbers: 96.50.Ci, 52.35.Ra

Introduction.—Temporal power spectra constructed from single spacecraft measurements of magnetic or velocity field fluctuations in the solar wind suggest that the solar wind plasma is in a stationary highly turbulent state whose energy spectrum $P(k)$ exhibits an inertial and a dissipation range [1–4]. Many *in situ* spacecraft observations have been showing that the inertial range has a spectral slope close to Kolmogorov's prediction $P(k) \propto k^{-5/3}$ for incompressible, isotropic hydrodynamic turbulence [3,4]. In fact, it is not too surprising, as at the distance of 1 AU there is sufficient time for the turbulence to evolve into stationarity. This is not anymore the case when the solar wind develops into shock waves, which happens near planetary bow shocks, coronal mass ejections, and corotating interaction regions. The best accessible of all those shocks is the Earth's bow shock, which evolves in the super-Alfvénic solar wind with Mach number typically 8–10 when it encounters the dipolar geomagnetic field. It forms a nearly parabolic shield in the solar direction at a geocentric distance of 11–14 Earth radii [5]. This supercritical collisionless shock distorts the solar wind by reflecting a substantial part of the incoming plasma back into the solar wind along the interplanetary magnetic field. Interaction between the two oppositely directed plasma streams causes various waves and instabilities through the ion beam instabilities [6]. Furthermore, the excited waves may interact with one another through parametric instabilities (decay and modulational instabilities), generating an ever-growing number of waves [7]. Such processes lead to the formation of an extended foreshock region in front of the quasiparallel shock where the magnetic and the velocity fields become highly oscillatory and both observations and simulations indicate that these shocks are constantly reforming [8,9]. Whether the foreshock reaches a turbulent state exhibiting a power-law scaling of the energy spectra can be answered by determining wave-number spectra $P(\mathbf{k})$. This is done in the present Letter for magnetic field fluctuations in the foreshock based on four-spacecraft Cluster magnetic field measurements [10,11]. The multipoint measurements in space allow us to *directly* determine the wave-number spectra and their anisotropy.

Wave-number spectra.—The magnetic field fluctuations are measured by Cluster spacecraft with a 22 Hz sampling frequency for the time interval 0805–0833 UT on 18 February 2002, when Cluster was in the terrestrial foreshock. The accessible wavelength range is limited by the spacecraft separation (down to about 100 km). The plasma parameter β is about 3.4. Figure 1 displays the recorded parallel and perpendicular magnetic field fluctuations with respect to the mean field direction. Amplitudes are about 5 nT in the both components, while some spiky signals reach the same order as the ambient field strength, 10 nT.

The wave-number spectra analysis makes extensive use of the *wave telescope* method developed particularly for application to multispacecraft missions like Cluster. It provides a representation of a measured finite amplitude wave field as an ensemble of propagating plane waves [12–14] and determines a (3 by 3) spectral energy density matrix $\mathsf{P}(\omega, \mathbf{k}) = \langle \mathbf{b}(\omega, \mathbf{k}) \mathbf{b}^{\dagger}(\omega, \mathbf{k}) \rangle$ for the magnetic field fluctuation amplitude $\mathbf{b}(\omega, \mathbf{k})$ at frequency ω and wave vector $\mathbf{k}$, retaining the phase information. (The dagger † denotes Hermitian conjugate.) Its diagonal elements represent spectral energy density (or simply power) in the x, y, and z directions, for example, parallel and perpendicular to the ambient field, and its trace $P = \mathrm{Tr}\mathsf{P}(\omega, \mathbf{k})$ yields total power. The task is to find the best estimator for P using the measured fluctuations $\mathbf{b}(\omega, \mathbf{r}_s)$ at positions $\mathbf{r}_s$ of the spacecraft. The optimal expression is given as [12,14]

$$\mathsf{P} = [\mathsf{H}^{\dagger}(\mathbf{k}) \cdot \mathsf{M}^{-1}(\omega) \cdot \mathsf{H}(\mathbf{k})]^{-1}, \quad (1)$$

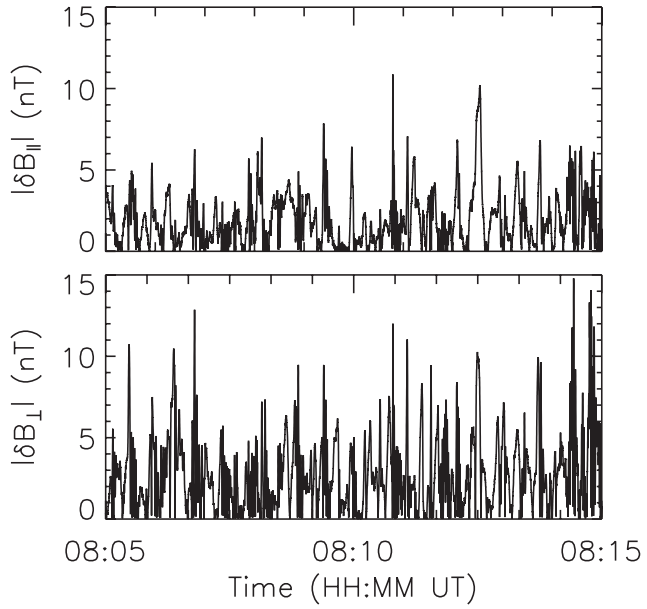

FIG. 1. Magnetic field fluctuations exhibiting burstlike small scale fluctuation recorded by Cluster 1 on 18 February 2002. Time unit is given with hours and minutes (HH:MM) in universal time (UT).

where the measured magnetic fluctuations are contained in the 12 by 12 covariance matrix $\mathsf{M}(\omega) = \langle \mathbf{B}(\omega)\mathbf{B}^{\dagger}(\omega)\rangle$, with $\mathbf{B}(\omega) = [\mathbf{b}(\omega, \mathbf{r}_1), \ldots, \mathbf{b}(\omega, \mathbf{r}_4)]^T$ and $\mathsf{H}(\mathbf{k}) = [\mathsf{I}e^{i\mathbf{k}\cdot\mathbf{r}_1}, \ldots, \mathsf{I}e^{i\mathbf{k}\cdot\mathbf{r}_4}]$. ($\mathsf{I}$ denotes the 3 by 3 unit matrix.) Deriving expression (1) requires constructing a suitable projection procedure that eliminates all signal contributions (or noise) that do not correspond to a given $\mathbf{k}$; that is, one needs to consider

$$\mathsf{P} = \mathsf{w}^{\dagger}(\mathbf{k}) \cdot \mathsf{M}(\omega) \cdot \mathsf{w}(\mathbf{k}) \tag{2}$$

with the constraint

$$\mathsf{w}^{\dagger}(\mathbf{k}) \cdot \mathsf{H}(\mathbf{k}) = \mathsf{I}, \tag{3}$$

where $\mathsf{w}(\mathbf{k})$ is a weight matrix that has to be determined. Minimizing the trace of P under this constraint yields the estimator (1) that minimizes the noise [14]. Having 4 point measurements, the spectral analysis is extended from the frequency domain to the wave-number domain. Determination of reliable wave numbers and their associated powers consists in a search for peaks in the power distribution in the wave-number space at which the noise of the power is minimized to zero. For example, if there is no specific wave mode present, i.e., if white noise is investigated, the wave telescope finds a flat distribution of the power in the $(\omega, \mathbf{k})$ space, and no wave mode is identified.

The covariance matrix $\mathsf{M}(\omega)$ is first determined by averaging over 16 time subintervals in the mean magnetic field aligned coordinate system (with the z axis parallel to the mean field) at frequencies up to 5 Hz. Then the spectral energy density matrix P is determined at wave numbers up to 0.04 km^{-1} in various directions with the angle resolution 10°. The limit in the analyzed frequency and the wave number is chosen to avoid spatial aliasing in the power distribution. We impose a further condition for clearer signals, namely, the signal-to-noise ratio (S/N) $p_{\max}/p_{\mathrm{mean}} > 3$, where $p_{\max}$ and p_{mean} denote the peak power and the angle-averaged power, respectively.

Figure 2 (top panel) displays the frequency-integrated total power in the wave-number domain. Interestingly, the spectrum exhibits some ranges that are reminiscent of turbulence. First, it peaks at smaller wave numbers about $k = 1.3 \times 10^{-3}$ km^{-1}. Second, the spectral curve shows an almost power-law decay toward larger wave numbers, which is characteristics to a turbulence inertial range spectrum. Third, the spectral slope becomes sharper when it crosses wave numbers about $k = 2.0 \times 10^{-2}$ km^{-1}, suggesting that the dissipation effect is operating and the energy is transformed into heat. Typical ion dynamics scales are displayed in Fig. 2 as well. Thermal ion gyro-wave-number k_{gy} is almost in the middle of the inertial range ($k_{\mathrm{gy}} = v_{\mathrm{th}\perp}/\Omega_i = 7.3 \times 10^{-3}$ km^{-1}). The ion inertial length wave number k_{in} is larger than k_{gy} ($k_{\mathrm{in}} = \omega_i/c = 1.3 \times 10^{-2}$ km^{-1}), and slightly smaller than the

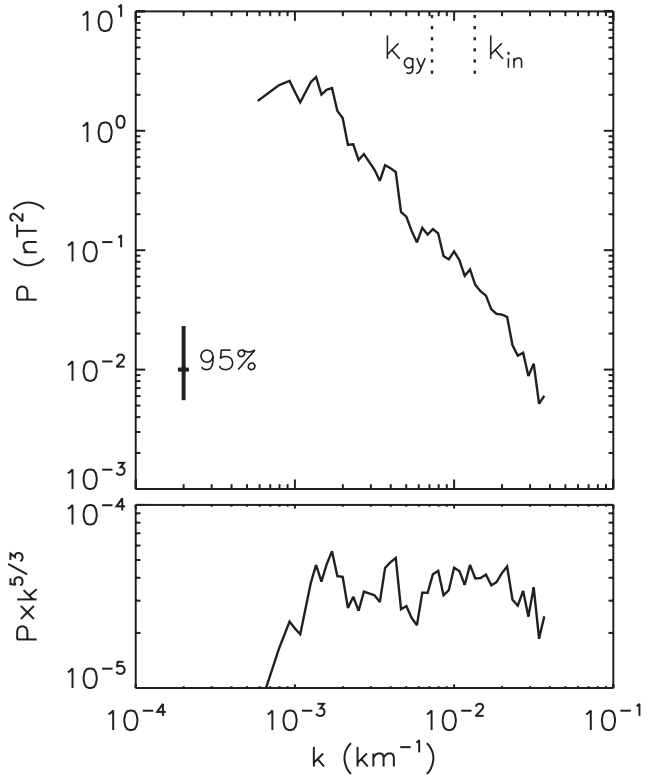

FIG. 2. Total power as a function of wave-number magnitude k. The wave numbers corresponding to ion gyroradius (k_{gy}) and ion inertial length (k_{in}) are also displayed. The vertical bar on the left denotes the confidence interval of the wave power for 95% reliability with 16 degrees of freedom, and the horizontal bar is the grid size in the wave-number space (equidistant in logarithmic scale).

scale where the dissipation starts. Above, Ω_i and ω_i denote the ion cyclotron frequency and the ion plasma frequency, respectively, $v_{\mathrm{th}\perp}$ the perpendicular ion thermal velocity, and c the speed of light. Although the scatter of the powers does not allow a unique identification of the power-law index α (assuming $P \propto k^{-\alpha}$), the mean spectral curve can be approximated with $\alpha = 5/3$, as the compensated spectrum exhibits an almost horizontal line (bottom panel).

Using the spectral density matrix P it is furthermore possible to determine anisotropy of the wave-number spectra, for example, to examine if an isotropic energy distribution which is often assumed in turbulence models is justified. Note that the divergence-free nature of the magnetic field $\nabla \cdot \mathbf{B} = 0$ implies that the wave vectors and the magnetic field fluctuations must be strictly orthogonal to each other. Hence the compressive power $P_\parallel$ depends on $k_\perp$ (wave number perpendicular to the magnetic field) and vice versa.

Figure 3 (top panel) displays the wave-number spectrum for the noncompressive (solenoidal) fluctuations ($P_\perp = P_{xx} + P_{yy}$), where the x and y directions are perpendicular to the ambient magnetic field. To enhance the quality of the spectrum, the same S/N condition as the total power case is imposed for $P_\perp$, too. It is found that the noncompressive spectrum bears most of the power; i.e., the noncompressive power is the same order as the total power. The spectral curve peaks almost at the same wave number as the total power spectrum ($k_\parallel = 1.3 \times 10^{-3}$ km^{-1}) and exhibits the power-law decay which can also be approximated with $\alpha = 5/3$ (bottom panel). The dissipation range can also be seen at larger wave numbers ($k_\parallel \geq 2.0 \times 10^{-2}$ km^{-1}), which are slightly larger than k_{in}.

Figure 4 (top panel) displays the compressive spectrum ($P_\parallel = P_{zz}$) as function of $k_\perp$ under the same S/N condition as above. The powers are smaller than the noncompressive ones by almost 1 order of magnitude at various wave numbers. There is no clear energy injection nor dissipation range visible in the spectrum. Furthermore, the spectral slope becomes flatter toward larger wave numbers and the identification of the inertial range is thus difficult. Nevertheless, we note that the power-law index can still be roughly approximated with $\alpha = 5/3$ (bottom panel).

Self-similarity.—As Fig. 1 indicates, there are large amplitude spiky signals in the fluctuations. They appear also as tails in probability distribution functions (PDFs) of the fluctuation amplitudes. For instance, if the fluctuation pattern is self-similar and does not exhibit any spikes, the PDF takes the form of Gaussian distribution. The PDFs of the measured field are displayed in Fig. 5, where the fluctuations δB about the mean field have been binned at 0.01 nT disturbance levels for all four spacecraft and normalized to their respective standard deviations. Here,

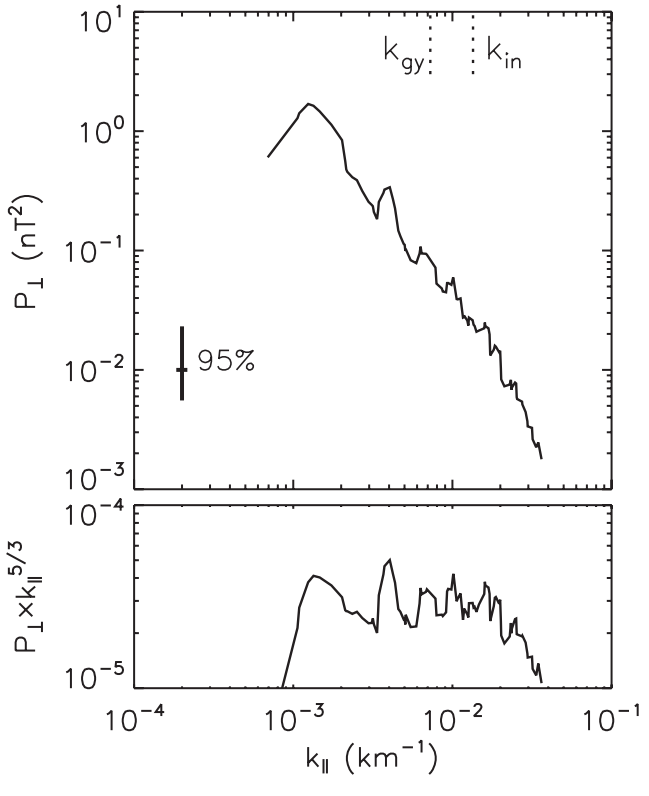

FIG. 3. Spectral energy density of noncompressive fluctuations ($P_\perp$) as function of wave number parallel ($k_\parallel$) with respect to the ambient magnetic field (top panel) and compensated spectrum with $\alpha = 5/3$ (bottom panel).

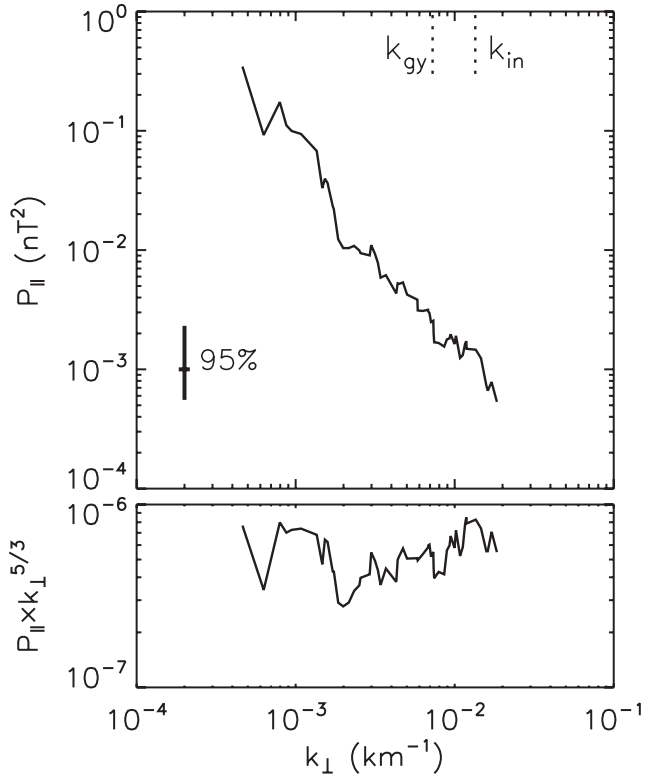

FIG. 4. Spectral energy density of compressive fluctuations as function of perpendicular wave number (top panel) and compensated spectrum with $\alpha = 5/3$ (bottom panel).

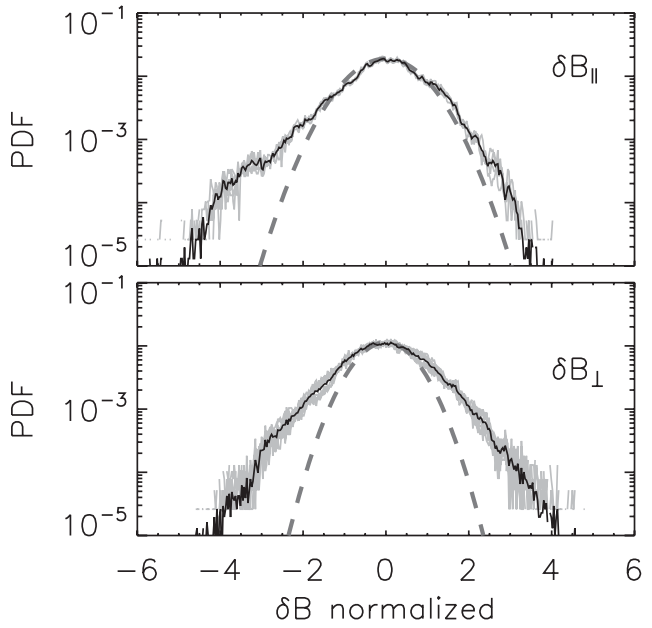

FIG. 5. Probability distribution functions (PDFs) of the magnetic fields for the compressive ($\delta B_{\parallel}$) and the noncompressive ($\delta B_{\perp}$) parts. Solid curves in gray and black represent PDFs superposed for four s/c data and PDFs averaged over four s/c data, respectively. Dashed curves are the corresponding Gaussian-fit around $\delta B = 0$.

the mean field represents a linear fit of the time series data. The PDFs exhibit well-expressed non-Gaussian wings at large amplitudes and asymmetries in both the compressive and noncompressive components. A measure of non-Gaussianity is known as the kurtosis which is obtained from the fourth and the second order moments of the PDFs as $F_k = \langle(\delta B)^4\rangle/\langle(\delta B)^2\rangle^2$. In the present case, $F_k = 3.5$ and 4.6 for the compressive and the noncompressive components, respectively. (Compare a Gaussian distribution yields $F_k = 3$.) Non-Gaussianity is more prominent in the perpendicular direction.

Conclusions.—In short, the direct determination of the wave-number spectra suggests that the fluctuations are turbulencelike and characterized by the energy injection, the inertial, and the dissipation ranges. This is clearest in the total power spectra. In addition, the fluctuations are highly anisotropic and intermittent. The perpendicular powers (for parallel propagating waves) dominate in the spectra. The inertial range can be identified with the power-law index roughly $\alpha = 5/3$ in all three spectra. The dissipation range is visible in the total and the noncompressive power spectra, and its spatial scale is a little smaller than the ion inertial length.

The foreshock turbulence should not be regarded as strong turbulence, since the fluctuation amplitudes are smaller than the background field strength, but rather it seems to be a set of (parallel propagating) Alfvén waves with minor contributions from compressive (e.g., magnetosonic) waves. This favors the concept of weak turbulence. The energy cascade scenario seems to be applicable in the foreshock, such that the first waves are excited at smaller wave numbers most probably by the ion beam instabilities and they interact with one another, generating daughter waves, forming the inertial range spectrum. If the foreshock fluctuations are dominated by the wave-wave interactions, resonant conditions are satisfied for the frequencies and the wave numbers between the parents and the daughter waves. In such a case, phases of the interacting waves are not randomly distributed but they are coherent so that spikelike fluctuations grow at discrete spatial points, reaching the same order as the background field strength. This may explain the existence of intermittency in the foreshock.

This work was supported by the Federal Ministry for Education and Research (Bundesministerium für Bildung und Forschung) and the German Aerospace Center (Deutsches Zentrum für Luft- und Raumfahrt) under Contract No. 50OC0103. We thank A. Balogh for discussions, and H. Rème for providing Cluster ion data.

*Electronic address: y.narita@tu-bs.de
†Also at Max Planck Institute for Solar System Research, Katlenburg-Lindau, Germany.
‡Senior visiting scientist at International Space Science Institute, Berne, Switzerland.

[1] W. H. Matthaeus, M. L. Goldstein, and C. Smith, Phys. Rev. Lett. **48**, 1256 (1982).
[2] M. L. Goldstein and D. A. Roberts, Phys. Plasmas **6**, 4154 (1999).
[3] R. J. Leamon, C. W. Smith, N. F. Ness, and W. H. Matthaeus, J. Geophys. Res. **103**, 4775 (1998).
[4] S. D. Bale, P. J. Kellogg, F. S. Mozer, T. S. Horbury, and H. Rème, Phys. Rev. Lett. **94**, 215002 (2005).
[5] J. Merka, A. Szabo, T. W. Narock, J. H. King, K. I. Paularena, and J. D. Richardson, J. Geophys. Res. **108**, 6 (2003).
[6] S. P. Gary, *Theory of Space Plasma Microinstabilities* (Cambridge University Press, Cambridge, 1993).
[7] M. Hoshino and M. L. Goldstein, Phys. Fluids B **1**, 1405 (1989).
[8] D. Krauss-Varban and N. Omidi, J. Geophys. Res. **96**, 17 (1991); **96**, 715 (1991).
[9] Y. Nariyuki and T. Hada, Earth Planets Space **57**, e9 (2005).
[10] C. P. Escoubet, M. Fehringer, and M. Goldstein, Ann. Geophys. **19**, 1197 (2001).
[11] A. Balogh *et al.*, Ann. Geophys. **19**, 1207 (2001).
[12] K.-H. Glassmeier *et al.*, Ann. Geophys. **19**, 1439 (2001).
[13] K.-H. Glassmeier, Ann. Geophys. **21**, 1071 (2003).
[14] U. Motschmann, T. I. Woodward, K. H. Glassmeier, D. J. Southwood, and J. L. Pinçon, J. Geophys. Res. **101**, 4961 (1996).